Degradation of chlorobenzene by non-thermal plasma coupled with catalyst: influence of catalyst, interaction between plasma and catalyst

Xiujuan SHI (石秀娟)[1], **Wenjun LIANG** (梁文俊)[1,2,*], **Guobin YIN** (尹国彬)[1] and **Jia LIU** (刘佳)[1]

[1] Key Laboratory of Beijing on Regional Air Pollution Control, Beijing University of Technology, Beijing 100124, People's Republic of China
[2] State Environmental Protection Key Laboratory of Odor Pollution Control, Tianjin Academy of Eco-environmental Sciences, Tianjin 300191, People's Republic of China

E-mail: liangwenj@bjut.edu.cn

CrossMark

Abstract

Non-thermal plasma (NTP) is considered to be a promising technology for the removal of volatile organic compounds; however, its application is limited by low CO_2 selectivity and undesirable by-products. To overcome these issues, this paper discusses the degradation of chlorobenzene (CB) in systems of NTP coupled with catalysts, and the influence of catalyst locations in the NTP was investigated. In addition, the interaction between plasma and catalyst was also explored. The results indicated that the degradability of CB was remarkably improved through the combination of NTP with catalysts, and the formation of ozone was effectively inhibited. The degradation efficiency increased from 33.9% to 79.6% at 14 kV in the NTP-catalytic system, while the ozone concentration decreased from 437 to 237 mg m^{-3}, and the degradation efficiency of in plasma catalysis (IPC) systems was superior to that of the post plasma catalysis system, while the inhibition ability of ozone exhibited an opposing trend. In the IPC system, the degradation efficiency was 87.7% at 14 kV, while the ozone concentration was 151 mg m^{-3}. Besides, the plasma did not destroy the pore structure and crystal structure of the catalyst, but affected the surface morphology and redox performance of the catalyst. Thus, NTP coupled catalytic system could improve the degradation performance of CB. Furthermore, the plasma discharge characteristics played a major role in the NTP synergistic catalytic degradation of CB. Finally, based on the experiment analysis results, the general reaction mechanism of CB degradation in an IPC reaction system was proposed.

Keywords: non-thermal plasma, chlorobenzene, catalysts, ozone, decomposition mechanism

(Some figures may appear in colour only in the online journal)

1. Introduction

Volatile organic compounds (VOCs), a precursor for ozone and fine particulate matter, are volatile, widely sourced, and have complex compositions. They have received significant research attention due to their significant threat to human health and the environment [1–3]. As a type of VOC, chlorinated volatile organic compounds (CVOCs) have the characteristics of high toxicity, high stability, and low biodegradability [4–6]; further, as a typical CVOC, chlorobenzene (CB) is widely used in printing, petrochemicals and pesticides, which is a significant precursor of dioxins and

---

*Author to whom any correspondence should be addressed.

other highly toxic substances [7]. Therefore, it is necessary to take appropriate measures to control its emissions. Traditional methods, including adsorption [8], catalytic oxidation [9], and combustion technology [10, 11], have certain limitations in the treatment of low concentration VOCs [12, 13]. Further, non-thermal plasma (NTP) is considered to be one of the most promising technologies for the removal of VOCs, with the advantages of operating under normal temperature and pressure conditions, simple equipment, the simultaneous treatment of a variety of pollutants, and its capacity to be turned on at any time. Therefore, it is widely applied to the degradation of VOCs, especially low-and medium-concentration VOCs [14]. However, its application is limited owing to low CO_2 selectivity and the generation of undesirable by-products [15–17].

To overcome these issues, several researchers have combined NTP with catalysts and achieved satisfactory results [18]. However, in the plasma synergetic catalytic system, the influence of their combination mode on VOCs has attracted considerable research attention [19, 20]. According to the different placements of catalysts, systems can be divided into in-plasma catalysis (IPC) systems (catalysts are placed in the discharge area) and post-plasma catalysis (PPC) systems (catalysts are placed downstream of the discharge area). For IPC systems, the short-lived and long-lived substances produced during the discharge process could be captured by the catalyst; however, for PPC systems, only long-lived species can reach the catalyst surface [21]. In comparison to PPC systems, the interactions between plasma and catalysts in IPC systems can improve the degradation efficiency of VOCs, but will also produce undesirable by-products such as ozone [22]. Most studies have shown that the VOC degradation efficiency of IPC systems is better than that of PPC systems [23, 24]; however, some studies have reached contrasting conclusions [25]. Although some researchers have compared the work of IPC and PPC systems in VOCs degradation, few researchers have conducted a comprehensive study on the placement of catalysts in the reactor, exploring the impact of catalysts placed in the front, middle, and rear of the discharge area, outside the discharge area, and partially placed inside the discharge area and outside the discharge area on pollutant degradation performance and ozone generation.

In NTP coupled catalytic system, the choice of catalyst is of vital importance. Studies have indicated that in the degradation of VOCs, the formation of by-products and mechanisms varied slightly for different active component catalysts. The transition metal Mn is widely coupled with NTP due to its low cost, good low-temperature activity, multivalence, high oxygen storage capacity [26, 27] and good dispersion [28]. The research results of Liu *et al* [29] have proved that Mn-based catalysts have good performance in CB degradation. Furthermore, in IPC systems, there was direct contact between NTP and catalysts and many reactions occur. The introduction of a catalyst into the plasma reaction system would enhance the electric field strength in the reactor and accelerate the plasma catalytic reaction, while the NTP would affect the redox activity of the catalyst, providing more active

sites [30, 31]. Therefore, the interaction between NTP and catalyst would affect the plasma catalytic reaction process, which was of great significance for further understanding the mechanism of plasma catalytic reaction. However, now researchers mostly focus on the degradation performance of the system through the degradation efficiency, CO_x selectivity, and other indicators. The interactions between plasma and catalysts are rarely investigated, and their reaction mechanism needs to be further understood.

In this study, the CB degradation performance of γ-Al_2O_3 and MnO_x/γ-Al_2O_3 catalysts in NTP was investigated. The effects of the catalyst locations in the NTP were also discussed. The removal efficiency (RE), CO_2 selectivity, energy efficiency (EE), and ozone variation were used to ascertain the removal performance of CB in systems. To explore the interaction between the catalysts and plasma, not only the influence of catalyst introduction on reactor performance was investigated, but also various characterizations of fresh and used catalysts were carried out, including x-ray diffraction (XRD), N_2 adsorption–desorption, scanning electron microscope (SEM) analysis, Fourier transform infrared spectroscopy (FT-IR), x-ray photoelectron spectroscopy (XPS), and H_2 temperature-programmed reduction (H_2-TPR). Finally, the general reaction mechanism of CB degradation in IPC reaction systems was proposed based on the analysis results.

2. Materials and methods

2.1. Catalyst preparation

Herein, the catalyst was prepared using the impregnation method. According to previous experimental results and literature [32], it is clear that the degradation performance of a catalyst prepared using manganese acetate as a precursor is higher than that of manganese nitrate in plasma reactors. Therefore, the manganese acetate based catalyst was selected to carry out the experiments. The specific preparation method of the catalyst is as follows: with manganese acetate as the precursor, γ-Al_2O_3 pellets were used as the carrier to prepare the catalyst, that is, a certain concentration of manganese acetate solution was prepared and a certain mass of γ-Al_2O_3 pellets was added to the prepared precursor solution. After ultrasonic impregnation for 2 h, then the carrier was kept in the dark for 3 h, put into a water bath for heating treatment for 3 h, and finally dried at 110 °C for 3 h and calcined in air at 500 °C for 3 h.

2.2. Catalyst characterization

The crystal structure of the catalyst was analyzed through XRD (Bruker/AXS, Germany) equipped with Cu-Kα radiation, with a scanning speed of 5° min^{-1}, scanning step of 0.02°, and scanning range of $2\theta = 5°–90°$.

The composition and surface deposits of the catalyst were analyzed through FT-IR (Nicolet, Thermo Fisher Scientific, USA). The tested sample powder was mixed with
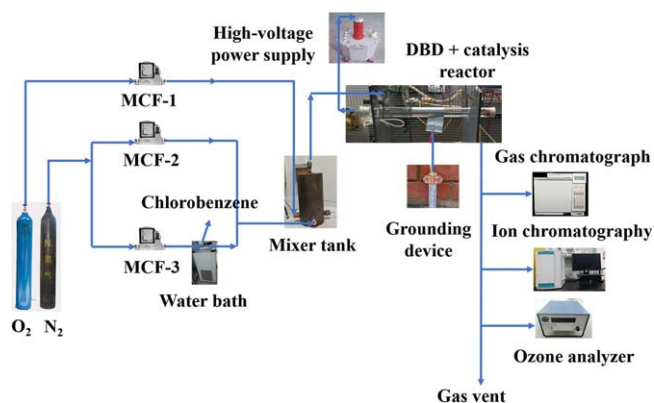
Figure 1. Schematic of the experimental setup.

Figure 2. Locations of the catalyst in the discharge area ((a): front end of the discharge area; (b): middle of the discharge area; (c): rear end of the discharge area; (d): outside the discharge area; (e): inner half discharge area and outer half discharge area).

dried KBr and then pressed into tablets for sample preparation. The spectrum collection range was 400–4000 cm^{-1}, the step length was 0.4 cm^{-1}, and the scanning times were 16.

The specific surface area (S_{BET}), average pore size (d_p), and total pore volume (V_p) of the catalysts were analyzed using a micromeritics ASAP 2050 automatic physical adsorption instrument in a liquid nitrogen ($-196\,^{\circ}C$) environment. Before the measurements, the samples were degassed in a vacuum at 250 $^{\circ}C$ for 2 h. And the morphology of catalysts was studied using SEM (Hitachi, SU 8220, Japan).

The surface charge of the catalysts was analyzed through XPS, using an ESCALAB 250XI (Thermo, USA) with Al-Kα radiation ($h\nu = 1486.8$ eV). All binding energies (BEs) were corrected by the C 1s binding energy value of 284.8 eV.

H_2-TPR experiments were performed on a 2920 automatic chemical adsorption instrument (Mike, USA) equipped with a thermal conductivity detector (TCD). Prior to analysis, 100 mg of the catalyst was pretreated for 1 h at 300 $^{\circ}C$ in an atmosphere of air; it was then cooled to room temperature, switched to an atmosphere of 10% H_2/Ar and purged for 30 min, after the baseline became stable. The reduction process was conducted by heating the catalyst from room temperature to 800 $^{\circ}C$ at a heating rate of 10 $^{\circ}C$ min^{-1}.

2.3. Experimental setup

This experiment was carried out under normal temperature and pressure conditions. As shown in figure 1, the experimental setup consisted of a reaction gas distribution system, DBD reactor, AC high voltage power supply system, and analysis system.

The bubbling method was adopted for producing CB. The background gas was prepared with nitrogen and oxygen, where nitrogen was divided into two paths: one path was pumped into the bubble bottle containing CB, and the CB molecules were volatilized into the mixing tank through water bath heating under constant temperature conditions; the other path directly entered the mixing tank, causing the oxygen to directly enter the mixing tank. The three-way gas finally entered the DBD reactor after being evenly mixed. Three-way air flows were controlled by three mass flow controllers (MFC, MIC20-series, JES, China), and the total gas volume
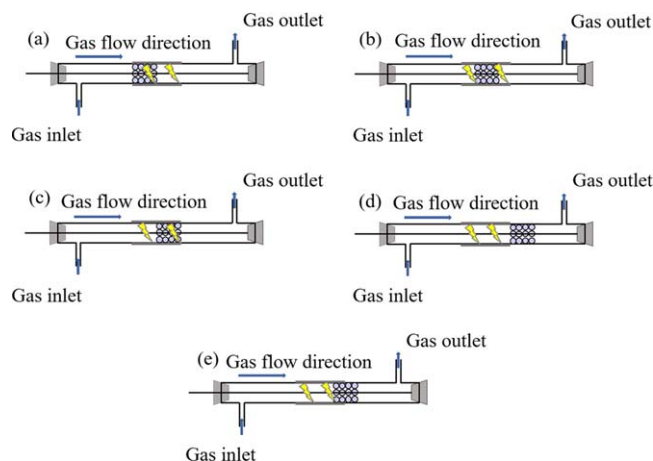
was controlled at 5 l min^{-1}. The experiment adopted the continuous method to determine the concentration of CB, that is, the gas flow containing CB continuously passed through the reaction tube equipped with catalysts, and continued to flow after the catalysts reached adsorption saturation. The inlet concentration of CB was determined after it remained relatively stable for 30 min. In this paper, the initial concentration of CB was controlled at 500 mg m^{-3}.

The DBD reactor adopted a coaxial tube structure and the material was quartz glass; its outer diameter and inner diameters were 32 mm and 29 mm, respectively. The high-voltage electrode was tungsten wire with a diameter of 1.25 mm, and aluminium foil was used as the grounding electrode. NTP was generated in the DBD reactor with an AC power supply (HTYD-10, Wuhan Sanxin Huatai Electrical Testing Equipment Co., Ltd, China). In early experiments, the catalyst was placed in the middle of the discharge area. In subsequent experiments, the effect of different locations of catalysts in the discharge area on the degradation of CB was explored. The specific locations of the catalysts are illustrated in figure 2.

The concentration of CB was analyzed using a gas chromatography (Agilent 6890N, USA) instrument equipped with an FID detector, which adopted an HP-5 capillary column (30 m × 320 μm × 0.25 μm), and the specific working conditions were as follows: oven temperature of 100 $^{\circ}C$, inlet temperature of 140 $^{\circ}C$, detector temperature of 200 $^{\circ}C$. The concentration of CO_2 was detected via gas chromatography (Agilent 6890N, USA) with the TCD detector, which adopted a capillary column (30 m × 530 μm × 40 μm), and the specific working conditions were as follows: oven temperature of 60 $^{\circ}C$, inlet temperature of 100 $^{\circ}C$, detector temperature of 200 $^{\circ}C$. The off-gas was injected into 0.01 mol l^{-1} NaOH solution at the rate of 1 l min^{-1} for 30 min to absorb inorganic chlorine, and the solution was determined by anion chromatography (883 Basic IC plus, Metrohm). The NO_x was qualitatively analyzed by a Fourier-transform infrared spectroscopy (FTIR, Thermo Fisher Scientific). FTIR was performed at a resolution of 0.4 cm^{-1}. The gas cell's light
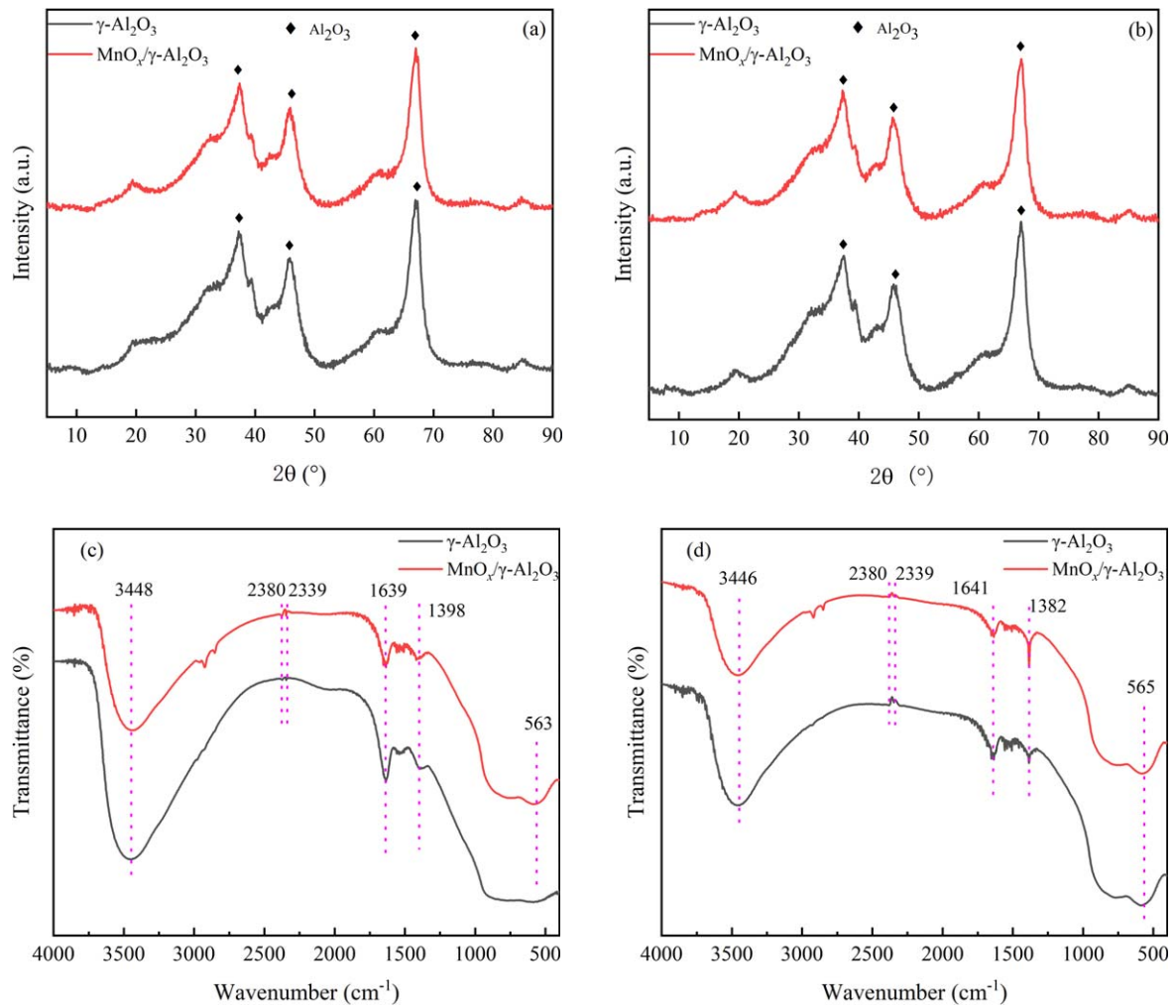
Figure 3. XRD ((a) fresh catalyst, (b) used catalyst) and FT-IR ((c) fresh catalyst, (d) used catalyst) spectra analysis.

pathway length was 2.4 m and the temperature was set as 150 °C during the analysis procedure. The concentration of ozone in the reaction process was determined using an ozone analyzer (106-M, 2B Technology), which was a significant product generated in the process of air plasma generation.

2.4. Evaluation method

The degradation performance of CB was determined using the removal efficiency (RE: %), specific energy density (SED: J l^{-1}), energy efficiency (EE: g kW^{-1} h^{-1}) and CO_2 selectivity (S_{CO_2}: %), which are calculated as follows:

$$RE(\%) = \frac{C_{in} - C_{out}}{C_{in}} \times 100\% \qquad (1)$$

$$SED \ (J \ l^{-1}) = \frac{U_{max} I}{\sqrt{2} Q} \times 60 \qquad (2)$$

$$EE \ (g \ kW^{-1} h^{-1}) = \frac{C_{in} - C_{out}}{SED} \times 3.6 \qquad (3)$$

$$S_{CO_2} \ (\%) = \frac{[C_{CO_2}]_{out}}{6 \times (C_{in} - C_{out})} \times 100\%, \qquad (4)$$

where C_{in} is the initial concentration of CB, mg m^{-3}; C_{out} is the outlet concentration of the CB after DBD treatment, mg m^{-3}; $C_{CO_2\text{-out}}$ is the CO_2 concentration at the reactor outlet, mg m^{-3}; Q is the gas flow rate, l min^{-1}; U_{max} is the discharge voltage, kV; and I is leakage current, mA.

3. Results and discussions

3.1. Characterization of catalysts

3.1.1. XRD analysis. X-ray diffraction (XRD) was used to detect the crystalline phase structure of the catalyst samples. The crystalline structures of the γ-Al_2O_3 and MnO_x/γ-Al_2O_3 fresh and used catalysts were studied by XRD, the results are shown in figures 3(a) and (b). Figure 3(a) depicts the XRD spectra of the fresh catalyst. It can be seen that the three main diffraction peaks at $2\theta = 37.5°$, $45.7°$, and $66.6°$ can be attributable to the cubic spinel structure of γ-Al_2O_3 (PDF#50-0741). The introduction of the active component Mn did not destroy the crystalline form of the γ-Al_2O_3 carrier, and the three main diffraction peaks of the MnO_x/γ-Al_2O_3 catalyst were slightly lower than those of the γ-Al_2O_3 carrier due to the interaction of MnO_x with the γ-Al_2O_3 carrier [33]. However, it can be seen that there was no MnO_x diffraction peak in the MnO_x/γ-Al_2O_3 catalyst according to the XRD
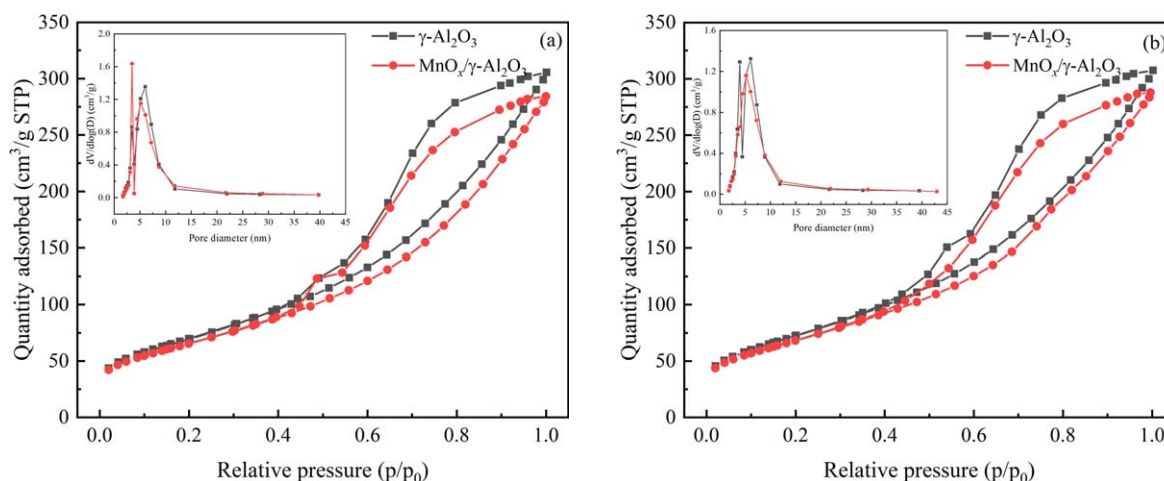
Figure 4. N_2 adsorption–desorption curve and pore size distribution of different catalysts ((a) fresh catalyst, (b) used catalyst).

Table 1. Specific surface area, total pore volume and average pore size of the fresh and used catalysts.

Catalyst sample	BET surface area S_{BET} ($m^2\ g^{-1}$)	Total pore volume V_p ($cm^3\ g^{-1}$)	Average pore size d_p (nm)
γ-Al$_2$O$_3$-fresh	257	0.48	7.55
γ-Al$_2$O$_3$-used	265	0.49	7.33
MnO$_x$/γ-Al$_2$O$_3$-fresh	238	0.45	7.61
MnO$_x$/γ-Al$_2$O$_3$-used	249	0.46	7.39

spectra. Combined with FT-IR spectra of MnO$_x$/γ-Al$_2$O$_3$ catalyst analysis (as shown in figures 3(c) and (d)), the Mn–O bond vibration peak observed in the catalyst proved that MnO$_x$ successfully loaded on the γ-Al$_2$O$_3$ carrier, indicating that Mn had good dispersibility on the γ-Al$_2$O$_3$ carrier under the condition of a low load. Furthermore, the XRD spectra of the used catalysts were measured (as shown in figure 3(b)), and compared with those of the fresh catalyst; the diffraction peak of each component in the catalyst samples did not change significantly, which proved that the discharge did not change the crystal structure of the catalyst [34].

3.1.2. FI-IR analysis. The FT-IR spectra for the fresh and used catalysts are shown in figures 3(c) and (d). The bands at 3450 and 1640 cm^{-1} of the fresh and used catalysts can be attributed to the O–H stretching vibration and O–H bending vibration, respectively, which indicates the presence of OH groups on the catalyst surface [35–37]. It has been demonstrated in previous studies that OH groups play an important role in the degradation process of VOCs [38]. The weak absorption peak of the fresh and used catalysts at 2300 cm^{-1} was caused by the anti-stretching vibration of CO$_2$. In comparison to the absorption peaks around 1400 cm^{-1} for the fresh and used catalysts, it can be seen that the vibration intensity of the used catalyst increases, which indicates that some carbonate substances may be formed by the combination of intermediate products and the catalyst during the reaction. For metal oxides, the infrared

correlation peaks were in the region below 1000 cm^{-1}. The peak near 565 cm^{-1} was the Mn–O vibration peak in the MnO$_6$ octahedral skeleton, which indicated the formation of Mn–O bonds [39, 40]. The FT-IR spectra of the catalyst indicated that MnO$_x$ was successfully loaded on the surface of the support.

*3.1.3. Analysis of N$_2$ adsorption–desorption performance.* Figure 4 shows the results of the N$_2$ adsorption–desorption isotherms and pore size distributions of the γ-Al$_2$O$_3$ and MnO$_x$/γ-Al$_2$O$_3$ catalysts for the fresh (figure 4(a)) and used (figure 4(b)) samples, and table 1 summarizes the specific surface areas (S_{BET}), total pore volume (V_p) and average pore size (d_p).

It can be clearly seen from figure 4 that all catalysts had typical type IV isotherms and H3 type hysteresis loops between P/P_0 at 0.4–1.0 for all the samples, indicating the presence of a typical mesoporous structure in all of the catalysts according to the IUPAC classifications [41–43]. Further, the hysteresis loops closed at low relative pressures, indicating that there are small mesopores in the catalyst. The pore size distribution curves were determined using the Barrett–Joyner–Halenda (BJH) method. The pore size of the packed material was concentrated in the range of 2.5–10 nm, and the most probable pore size was between 6 and 7 nm, which also indicates that there are small mesopores in the catalyst. In comparison with the fresh catalyst, the N$_2$ adsorption–desorption isotherms and pore-size distributions of the used catalyst did not differ significantly, indicating that the pore structure of the catalyst was not damaged during the discharge process.

The S_{BET} values of γ-Al$_2$O$_3$ and MnO$_x$/γ-Al$_2$O$_3$ were 257 and 238 $m^2\ g^{-1}$, respectively. This indicates that the introduction of active components made the catalyst surface wrinkled or filled with pores (as shown in SEM analysis), resulting in the reduction of the S_{BET} for MnO$_x$/γ-Al$_2$O$_3$ catalyst. According to the data on CB degradation activity, the relationship between the RE of CB and S_{BET} was not linear. In comparison to the MnO$_x$/γ-Al$_2$O$_3$ catalyst, although the S_{BET} of γ-Al$_2$O$_3$ was larger, its degradation efficiency of CB

Table 2. XPS characterization results of the fresh and used Mn based catalysts.

Catalyst sample	BE (eV)			BE (eV)		
	Mn^{4+}	Mn^{3+}	Mn^{4+}/Mn^{3+}	O_{latt}	O_{ads}	O_{latt}/O_{ads}
MnO_x/γ-Al_2O_3-fresh	643.55	641.71	0.88	529.33	530.85	3.91
MnO_x/γ-Al_2O_3-used	643.77	641.76	0.65	529.25	530.85	5.19
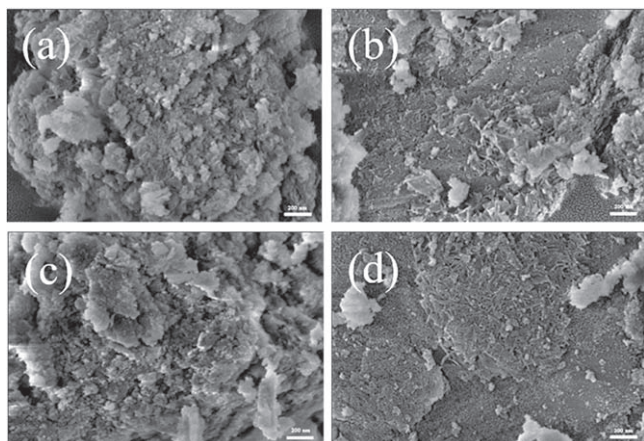
Figure 5. SEM images of catalysts for γ-Al_2O_3 ((a) fresh, (b) used) and MnO_x/γ-Al_2O_3 ((c) fresh, (d) used).

was not the best (as shown in figure 8(b)). This shows that, although a large S_{BET} was conducive to the physical adsorption of CB [44], it was not the only factor affecting the catalytic activity in the discharge process. After plasma treatment, the catalyst surface became refined, and the dispersion was relatively uniform. Therefore, the S_{BET} and V_p of the catalyst increased, and the d_p decreased; however, the change was small. This result is basically consistent with the experimental results found in previous literature [45].

3.1.4. SEM analysis. To observe the surface morphology of the catalyst, scanning electron microscopy (SEM) was used. SEM images of catalysts for γ-Al_2O_3 ((a) fresh and (b) used) and MnO_x/γ-Al_2O_3 ((c) fresh and (d) used) are shown in figure 5. It is clear that the surface of the pure γ-Al_2O_3 pellet carrier has many cavities and large depressions, with obvious pore structure (as shown in figure 5(a)). The introduction of active components Mn made the surface of MnO_x/γ-Al_2O_3 catalyst become dense and relatively smooth, indicating that some pores on the surface of the carrier were blocked by active components; therefore, the S_{BET} and d_p of the catalyst decrease and increase, respectively (as shown in table 1). Further, the depression on the catalyst surface was occupied by the active components, thus increasing the number of active centers and relatively evenly dispersing them on the catalyst surface, which improved the degradation efficiency of CB. In comparison to the fresh catalyst, the surface of the used catalyst was fine and the dispersion was uniform; therefore, the S_{BET} of the catalyst increased, which shows that

the surface structure of the catalyst was improved via plasma discharge.

3.1.5. XPS analysis. The surface chemical status of the fresh and used MnO_x/γ-Al_2O_3 catalysts was investigated by XPS analysis. The XPS spectra and analysis results are shown in figure 6 and table 2, respectively. The XPS spectra of Mn $2p_{3/2}$ was displayed in figure 6(a). As shown in figure 6(a), asymmetric Mn $2p_{3/2}$ peaks can be observed in the fresh and used MnO_x/γ-Al_2O_3 catalysts. After fitting, they were decomposed into three peaks of about 640 eV, 641.7 eV, and 643.5–643.8 eV, which could be attributed to Mn^{2+}, Mn^{3+}, and Mn^{4+}, respectively, indicating that Mn elements in the fresh and used Mn catalysts exist in different valence states [46–48]. In the NTP synergistic catalytic system, oxygen in the background gas, ozone, electrons, and free radicals generated during discharge were mutually converted on the catalyst surface through Mn valence states, and participated in the VOCs degradation process, greatly improving the degradation efficiency of CB [49]. The XPS spectra of O 1s are shown in figure 6(b). The asymmetric O 1s XPS spectra of the fresh and used catalysts can be decomposed into three components, of which the component with a binding energy of 529.3 eV belonged to the surface lattice oxygen (O_{latt}) species, the component with a binding energy of 530.8 eV belonged to the surface adsorbed oxygen (O_{ads}) species, and the component with a binding energy of 532.3 eV belonged to the surface adsorbed water or carbonate species [50, 51]. In comparison to the fresh catalyst, the Mn^{4+}/Mn^{3+} and O_{latt}/O_{ads} of the used catalyst decreased and increased, respectively; that is, Mn^{4+}/Mn^{3+} decreased from 0.88 to 0.65, while O_{latt}/O_{ads} increased from 3.91 to 5.19 (as shown in table 2). Previous studies have shown that Mn^{4+} and O_{latt} are conducive to VOCs removal in the NTP system [32, 52]. Mn^{4+} can effectively decompose O_3 in the reaction system to generate active oxygen atoms. Therefore, the relative content of Mn^{4+} in the used catalyst decreased.

3.1.6. H$_2$-TPR analysis. To investigate the redox performance of the catalyst, H_2-TPR analysis was carried out, the results are shown in figure 7. It can clearly be seen that no reduction peak was found in the sample of γ-Al_2O_3, while the profile of the catalyst prepared by introducing the active component Mn showed different reduction peaks, implying the existence of different manganese species. The fresh MnO_x/γ-Al_2O_3 catalyst exhibited strong and wide reduction peaks at 277 °C and 348 °C, which corresponded to the reduction processes of $MnO_2 \rightarrow Mn_2O_3$ and
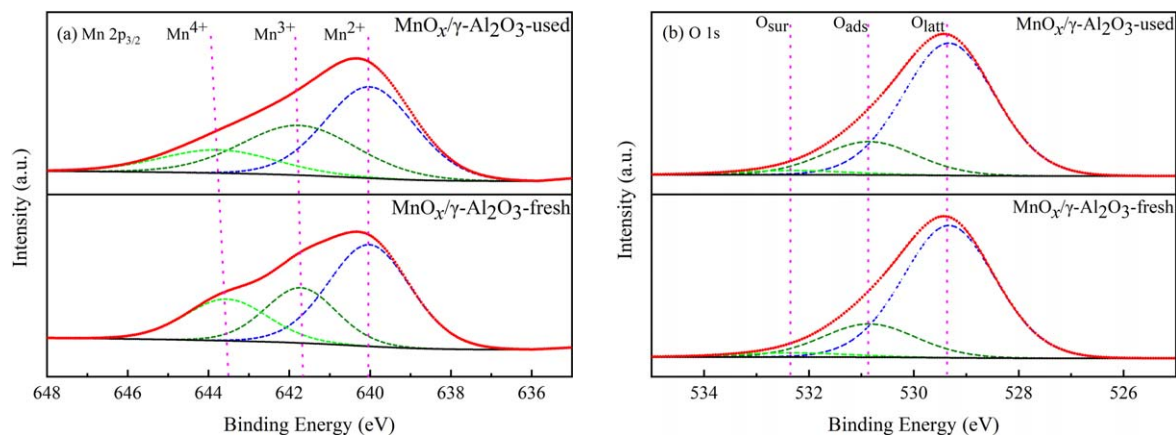
Figure 6. XPS spectra of Mn $2p_{3/2}$ (a) and O 1s (b) for the fresh MnO_x/γ-Al_2O_3 and used MnO_x/γ-Al_2O_3.
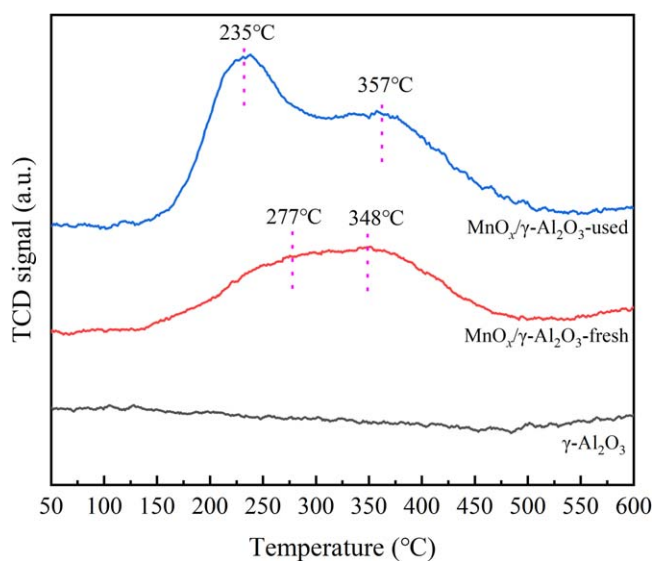
Figure 7. H_2-TPR curves of γ-Al_2O_3, fresh MnO_x/γ-Al_2O_3 and used MnO_x/γ-Al_2O_3.

$Mn_2O_3 \rightarrow MnO$, respectively [53–55]. This phenomenon indicates that the valence state of Mn in MnO_x/γ-Al_2O_3 is quite complex during the NTP synergetic catalytic process. In comparison to the fresh catalyst, the used MnO_x/γ-Al_2O_3 catalyst exhibited two reduction peaks, at 235 °C and 357 °C. Further, the reduction peak of $MnO_2 \rightarrow Mn_2O_3$ moved forward, and the reduction peak of $Mn_2O_3 \rightarrow MnO$ moved backwards and weakened through discharge treatment, indicating that the relative content of Mn^{4+} in the catalyst decreased, which was consistent with the XPS analysis results.

3.2. Degradation of CB by NTP synergistic catalysts

3.2.1. Effect of the catalyst on the degradation of CB.
The DBD reactor was applied to study the degradation of CB in an atmosphere of air. The effects of the discharge voltage and different catalysts on the RE, SED, and EE of CB were investigated, the results are shown in figures 8(a) and (b). It can be seen from figure 8(a) that the SED values of different

systems increased with the discharge voltage; however, the SED values of different systems presented differing trends. Under the same voltage conditions, the SED values are in the following order: NTP+MnO_x/γ-Al_2O_3 > NTP + γ-Al_2O_3 > NTP. In comparison to NTP alone, the SED of the reaction system increased through the introduction of catalysts. One possible reason for this is that the introduction of catalysts produces strong partial discharge under the action of an electric field, reducing the discharge gap in the NTP synergistic catalytic systems. Therefore, the SED of the systems was increased [34]. The SED of the system with MnO_x/γ-Al_2O_3 was higher than that of the system with γ-Al_2O_3, which was attributed to differences in the dielectric constant (ξ) for the catalysts. Further, it is known that the dielectric constant of γ-Al_2O_3 ranges from 9.34 to 11.54, while the dielectric constant of MnO_x was about 10^4; thus, the dielectric constant of MnO_x/γ-Al_2O_3 is greater than that of γ-Al_2O_3, and materials with a small dielectric constant do not have effective micro discharge between catalyst particles, resulting in decreases in the SED of systems [56].

As illustrated in figure 8(b), the introduction of the catalyst significantly improved the RE and EE of CB. The order of RE in terms of CB degradation is as follows: NTP+MnO_x/γ-Al_2O_3>NTP+γ-Al_2O_3>NTP under the same conditions. The system of NTP coupled with MnO_x/γ-Al_2O_3 obtained the optimum RE for CB degradation; however, there was no obvious law followed by the EE of the system, which was primarily due to the conversion of a portion of the energy into heat and light energy during the reaction process [57]. For example, the REs of CB for NTP alone, NTP+γ-Al_2O_3, and NTP+MnO_x/γ-Al_2O_3 were 33.9%, 67.4%, and 79.6%, respectively, at the discharge of 14 kV, while the EEs of CB were 2.4 g kw^{-1} h^{-1}, 2.8 g kw^{-1} h^{-1} and 3 g kw^{-1} h^{-1}, respectively. This was mainly attributed to the following reasons. Firstly, the catalysts in the reactor had a certain adsorption effect on CB, which prolongs its residence time in the reactor; further, the catalyst increases the dielectric constant of the system, which increases the RE of CB in the reaction system. Secondly, the introduction of catalysts also enhances the discharge intensity in the system, which promotes the ionization formation of high-energy active
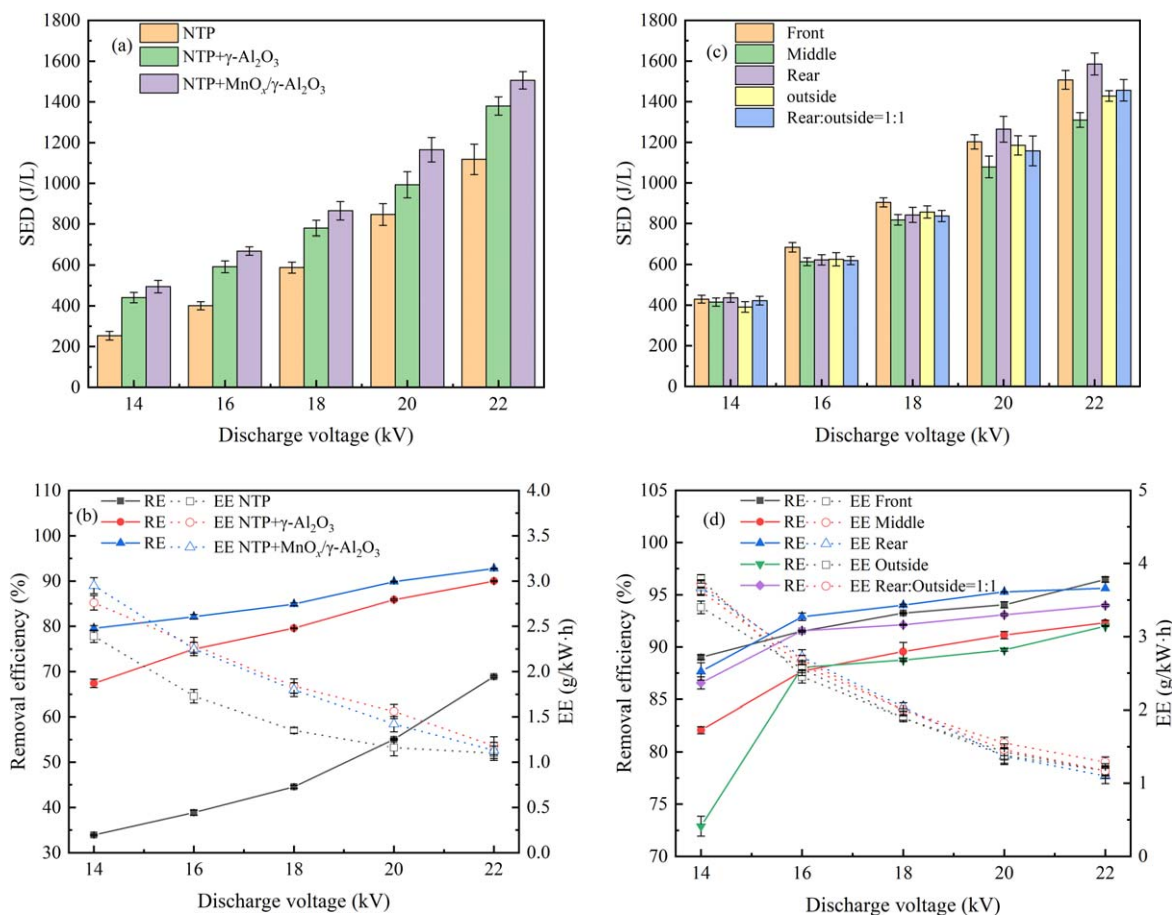
Figure 8. Effect of catalysts ((a) SED, (b) RE and EE) and locations of the catalyst in the NTP ((c) SED, (d) RE and EE) on the degradation of CB under different voltage conditions.

oxygen atoms and the transfer to a higher energy level [58]. This increases the temperature and energy level of the system and promotes the decomposition of ozone on the catalyst surface; the active oxygen atoms generated by decomposition participate in the CB degradation reaction, improving the RE and EE of CB degradation in the systems. Thirdly, in the system for NTP with $MnO_x/\gamma\text{-}Al_2O_3$, the oxygen in the background gas, ozone, electrons and free radicals generated during discharge are mutually converted on the catalyst surface through Mn valence states, and participate in the VOCs degradation process, greatly improving the degradation efficiency of CB [49].

$MnO_x/\gamma\text{-}Al_2O_3$ achieved the optimum RE value for CB under the same discharge voltage; with increase in the discharge voltage from 14 to 22 kV, the degradation efficiency increased from 79.6% to 92.8%. Increasing the discharge voltage led to the production of more active particles and high-energy particles in the reaction system, and the collision probability with CB increased; therefore, the degradation efficiency of CB improved. In comparison to only NTP, the degradation efficiency of CB for NTP with the $MnO_x/\gamma\text{-}Al_2O_3$ system increased by 45.7% under the conditions of 14 kV, while the degradation efficiency dropped to 23.9% at the discharge of 22 kV, which indicated that the introduction of catalysts could significantly improve the

degradation efficiency of CB under the condition of a low discharge voltage. Although the high-voltage condition provided more active particles for the reaction system and increased the collision probability between CB and active particles, a part of the energy of the systems was converted into light and heat energy [57]. The apparent temperature of the reactor reached 150 °C at 22 kV. As shown in figure 9, in comparison to the discharge voltage of 14 kV, spark discharge will occur during the discharge process of 22 kV, which will consume a significant amount of energy, resulting in a small increase in the degradation efficiency of CB in the system. Therefore, the addition of catalysts under high-voltage conditions has a small effect on improving the degradation efficiency of CB [59].

3.2.2. Effect of catalyst locations in the NTP on the degradation of CB. In NTP synergistic catalytic system, the different locations of the catalyst in the NTP had a significant influence on the degradation of CB. Therefore, it was necessary to investigate the impact of the locations of the catalyst in the NTP on the degradation performance of CB. In all kinds of reactors, the SED and RE of the systems increased when the applied voltage was increased from 14 to 22 kV, while the EE value exhibited a decreasing trend (as shown in figures 8(c)
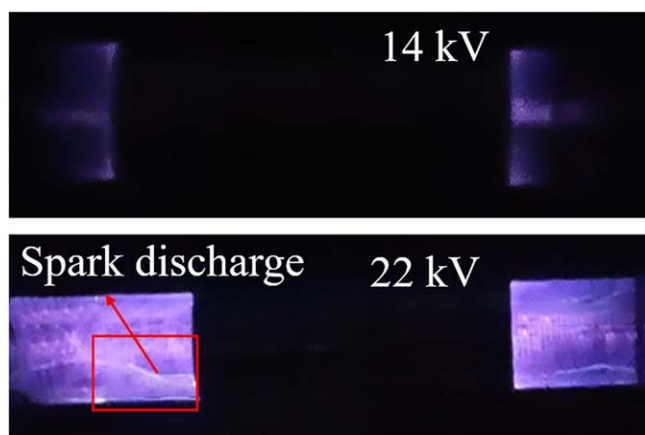
Figure 9. Images of the reactor at the discharge voltages of 14 and 22 kV.

and (d)). Further, more active substances were produced at higher voltages, resulting in more CB being degraded. However, more energy was converted into heat and light energy at higher voltages [57], which led to decreases in the EE of CB.

The RE of CB for the IPC (front, middle, and rear system) system exhibited small changes under the same voltage conditions, while the RE of the IPC system was higher than that of the PPC system throughout the discharge process. As such, the order of degradation efficiency of CB at 14 kV for each reaction system is as follows: front (89%) > rear (87.7%) > rear:outside (86.6%) > middle (82.1%) > outside (72.9%). The experimental results were consistent with those found in previous studies [23, 24, 60]. The reasons for this phenomenon were as follows. Firstly, in the IPC system, both long-lived (such as O_3) and short-lived species (O·, ·OH, and e) can be trapped on the catalyst surface to react with VOCs; however, in the PPC system, only long-lived species (such as O_3 and metastable particles) could reach the downstream catalyst [21]. Secondly, the existence of catalysts in IPC reactors affects the discharge intensity of plasma and improves its RE. However, in comparison to PPC reaction systems, the IPC reaction system has the limitation of higher ozone concentration [22]. The EE of the reaction system does not exhibit obvious regularity, which was mainly related to the energy consumption of these systems. According to the variations of the reactor's apparent temperature and the discharge image during the experiment, a portion of the energy generated in the discharge process was converted into heat and light energy.

3.3. By-product analysis

3.3.1. CO_2 selectivity. CO_2 selectivity can directly reflect the mineralization degree of the CB degradation process. The ideal degradation products of CB are H_2O, CO_2 and inorganic chlorine; however, the incomplete degradation of CB will produce many organic by-products. Figure 10 shows the

variation of CO_2 selectivity in different reaction systems at 14 and 22 kV.

As depicted in figure 10, in all reaction systems, the selectivity of CO_2 increased as the discharge voltage changed from 14 to 22 kV. This can be explained by increases in the active species at higher voltages, leading to more CB being degraded into CO_2 [17]. The effect of the different catalysts on the variation of CO_2 selectivity is illustrated in figure 10(a). In comparison to the NTP system, the introduction of γ-Al_2O_3 and MnO_x/γ-Al_2O_3 improved the CO_2 selectivity, and the reactor of MnO_x/γ-Al_2O_3 yielded the highest CO_2 selectivity, which was in the following order: NTP+MnO_x/γ-Al_2O_3 > NTP+γ-Al_2O_3 > NTP. The CO_2 selectivity of the system of NTP, NTP+γ-Al_2O_3, and NTP+MnO_x/γ-Al_2O_3 were 16.6%, 13.6%, and 26.1%, respectively, at 22 kV. This phenomenon could be explained by the following factors. Firstly, the introduction of the catalyst enhanced the discharge intensity of the reaction system (as shown in figure 8(a)), which increased the number of active particles (such as O· and ·OH); this is conducive to the further oxidation of CB in the system [61, 62]. In addition, the decomposition of ozone on the surface of Mn-based catalysts could also contribute to improving the CO_2 selectivity of the system (as illustrated in figure 11). The oxidizability of active oxygen atoms generated by ozone decomposition was higher than that of ozone [44, 63, 64], which could further oxidize the products of the system.

Figure 10(b) shows the effect of different locations of the catalyst in the NTP on the variation of CO_2 selectivity. For all reactors, the order of CO_2 selectivity was as follows: front (23.1%) < rear: outside = 1:1 (23.4%) < outside (23.9%) < middle (26%) ≈ rear (26.1%). In IPC systems, the CO_2 selectivity for the introduction of the catalyst into the middle and rear of the discharge area was higher than that of the front end, which was mainly related to the oxygen atoms produced by ozone decomposition. For the IPC system, the CO_2 selectivity was not only related to the active oxygen atoms, but was also affected by the active substances produced during the discharge process [65]. Therefore, in comparison to the PPC system, the CO_2 selectivity of the IPC system was relatively high. However, there was a small difference in CO_2 selectivity between IPC and PPC systems, and the research results were consistent with those of previous studies [20, 66].

3.3.2. Ozone and NO_x analysis. In the process of CB degradation by NTP in an atmosphere of air, ozone was an inevitable by-product. Although it was one of the important active substances for the degradation of CB in the NTP reactor, it was harmful to the environment. Therefore, the formation of ozone in different reaction systems was analyzed herein.

Figure 11 describes the variation of ozone content with discharge voltage in different systems. For all reaction systems, with increases in the discharge voltage, the ozone concentration exhibited a decreasing trend, reaching 0 at 22 kV. Throughout the discharge process, the introduction of the catalyst reduced the ozone concentration, and the order was NTP > NTP + γ-Al_2O_3 > NTP + MnO_x/γ-Al_2O_3. Ozone decomposed slowly
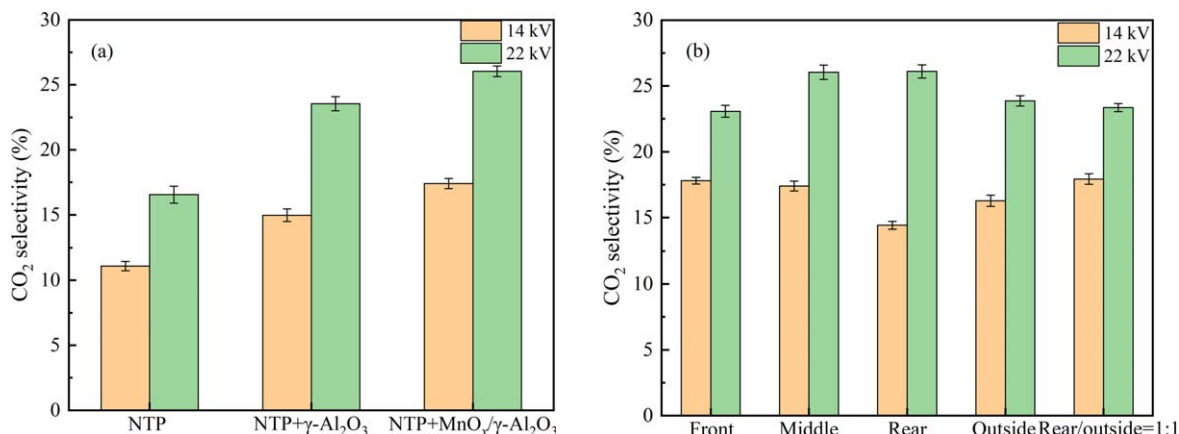
Figure 10. Selectivity of CO_2 in the NTP+catalysis reactor at 14 and 22 kV. (a) Effect of different catalysts; (b) effect of different locations of catalysts in the NTP.
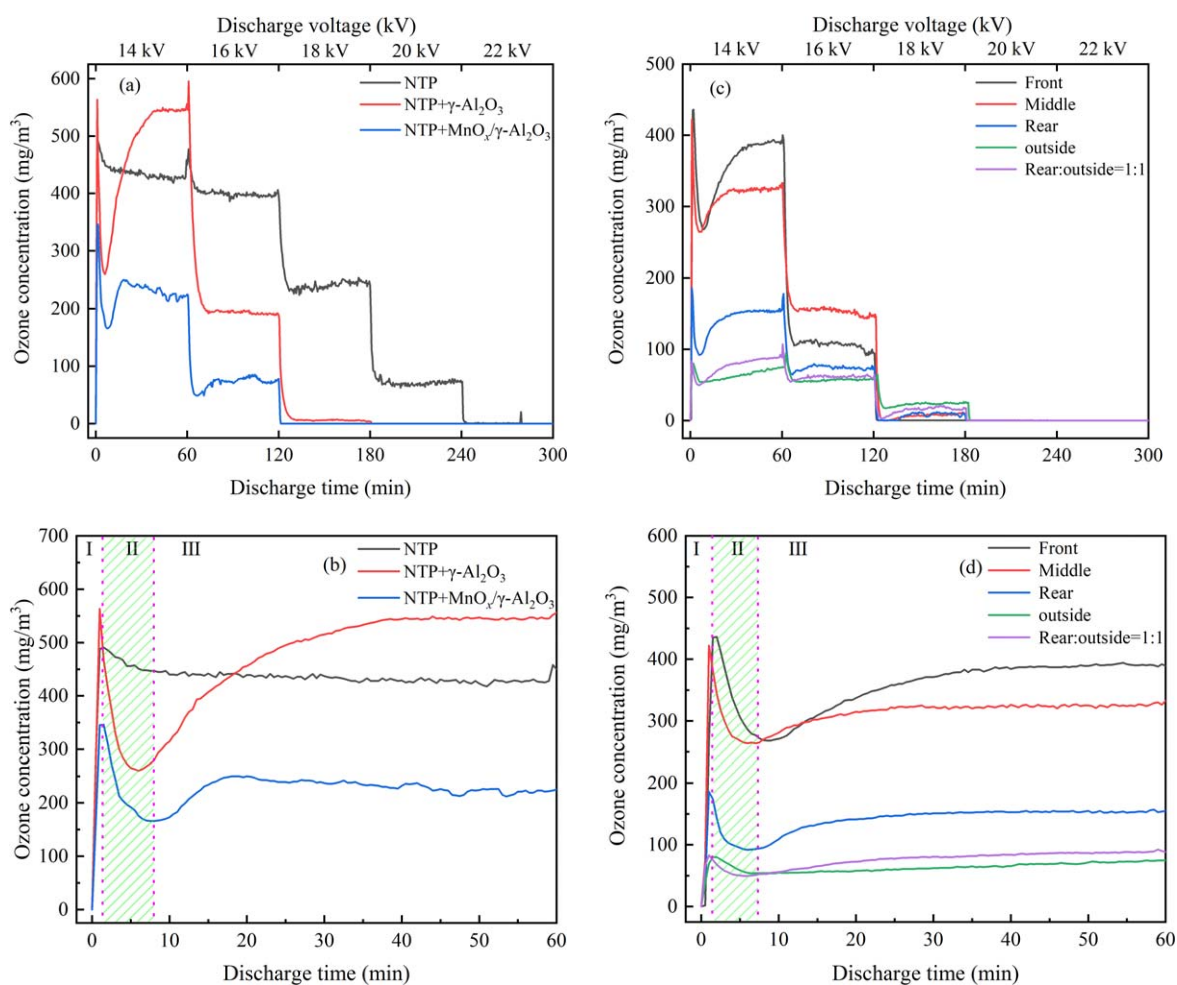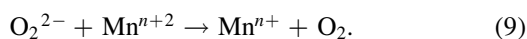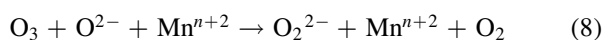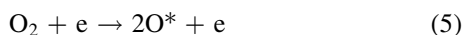

Figure 11. Effect of different catalyst ((a) and (b)) and different locations of catalysts ((c) and (d)) in the NTP on the variation of ozone in the reactor. (a) and (c) the variation of ozone in the entire process; (b) and (d) the variation of ozone at 14 kV.

at room temperature, while the increase in temperature especially above 100 °C could accelerate ozone decomposition. The introduction of catalysts enhanced the discharge effect and improved the temperature of the systems. The decomposition rate of ozone in the system was higher than the generation rate at temperatures above 100 °C, and the ozone concentration exhibits a decreasing trend overall [67]. For Mn-based catalysts,

ozone decomposed on the surface of the catalyst to generate active oxygen atoms [63, 64], which reduced the ozone concentration in the systems, and the active oxygen generated by ozone decomposition participated in the degradation of CB, which improved the degradation efficiency and EE of CB (as shown in figure 8(b)). The process of ozone generation and decomposition is reflected in equations (5)–(9) [27, 68]. As

shown in figure 11(c), the ozone concentration of IPC systems was higher than that of PPC systems. This is mainly attributed to the enhanced discharge effect of IPC systems, which produces more active particles, leading to the production of additional ozone. In terms of the degradation efficiency of CB, the IPC system was higher than the PPC system, which indicated that the degradation efficiency of CB for IPC systems could mainly be attributed to short-lived species, while that for PPC systems could mainly be attributed to ozone; therefore, PPC systems consume more ozone than IPC systems [20]

$$O_2 + e \rightarrow 2O^* + e \tag{5}$$

$$O^* + O_2 + M \rightarrow O_3 + M \tag{6}$$

$$O_3 + Mn^{n+} \rightarrow O^{2-} + Mn^{n+2} + O_2 \tag{7}$$

$$O_3 + O^{2-} + Mn^{n+2} \rightarrow O_2{}^{2-} + Mn^{n+2} + O_2 \tag{8}$$

$$O_2{}^{2-} + Mn^{n+2} \rightarrow Mn^{n+} + O_2. \tag{9}$$

For all reaction systems, the variation of ozone concentration was mainly divided into three stages (as shown in figures 11(b) and (d)) at the discharge voltage of 14 kV. The first stage was the stage of increasing ozone concentration, where the high-energy electrons produced by high-voltage discharge collided with O_2 in the reaction system to produce O·, and then combined with O_2 in the reaction system to generate ozone, resulting in an increasing trend of ozone concentration in the system. The reaction process is shown in equations (5) and (6). The second stage was the ozone decline stage. With the progression of the discharge reaction, the temperature increase of the reaction system led to the accelerated decomposition of ozone, and the decomposition rate of ozone was greater than its generation rate, resulting in an overall decline in ozone concentration. The third stage was the stationary stage of ozone. With the continuous increase of the discharge time, the temperature of the reaction system remained relatively stable, and the formation and decomposition of ozone in the reaction system remained basically constant in a relatively stable state, resulting in a stable trend of ozone concentration in the system as a whole.

In the process of NTP discharge, NO_x would inevitably be produced in the presence of air, including NO_2, NO and N_2O, etc. In this work, a simple qualitative analysis of the tail gas products from the degradation of CB by single NTP was carried out through FT-IR (as shown in figure 12). As can be seen from figure 12, under the condition of the different discharge voltages, only N_2O (2200 cm^{-1}) was determined by FTIR, while NO and NO_2 were not detected. This could be because NO and NO_2 were consumed immediately after being produced [12].

By analyzing the parameters of CB degradation efficiency, EE, CO_2 selectivity, ozone concentration, etc, it could be seen that the IPC system was better than the PPC system. Therefore, the interaction between the plasma of the IPC reaction system and catalyst and mechanism was analyzed.
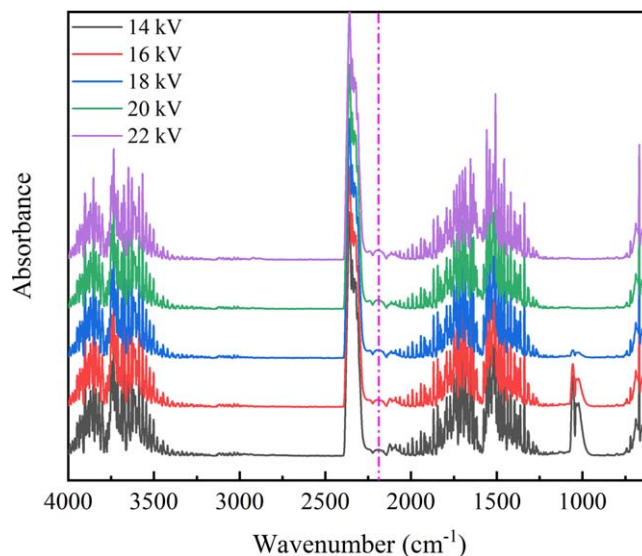

Figure 12. FT-IR spectra of exhaust gases from the system of non-thermal plasma degradation of CB.

3.4. Mechanism of the degradation of CB by NTP with a catalyst

3.4.1. Kinetics analysis of the degradation of CB by NTP with a catalyst. Kinetic analysis is an important measure to understand the rate and mechanism of a chemical reaction. However, it was difficult to directly measure and reasonably describe the concentration of active particles and reaction intermediates in a plasma catalytic system; therefore, the rate constants of physical and chemical reactions in a plasma catalytic system cannot be adequately determined. In addition, there is no complete model to comprehensively describe the complex interactions between plasma and the catalyst in an NTP coupled catalytic system, to the best of our knowledge [23, 49]. In a continuous plasma synergistic catalytic system, the internal and external diffusion and adsorption processes of reactants can be ignored owing to the short-lived active particles and short residence time. In this research, a simplified kinetic model was used to describe the reaction process of NTP coupled with catalysts for the degradation of CB. A plug flow in NTP systems was assumed, and the total reaction rate can be defined using equation (10) [69]. Plasma chemical reactions were affected by high-energy electrons, ions and active substances. On the basis that the initial concentration of the gas and gas volume were consistent, its generation was only related to the SED. Therefore, the total reaction rate can also be described using equation (11). Combining equations (10) and (11) leads to equation (12), which can be integrated with respect to the reaction time to yield equation (13). Finally, equation (14) can be acquired by combining equations (1) and (13)

$$\frac{dc_{CB}}{dt} = -R_{overall} \tag{10}$$

$$R_{overall} = k' \cdot c_{CB} \cdot SED \tag{11}$$

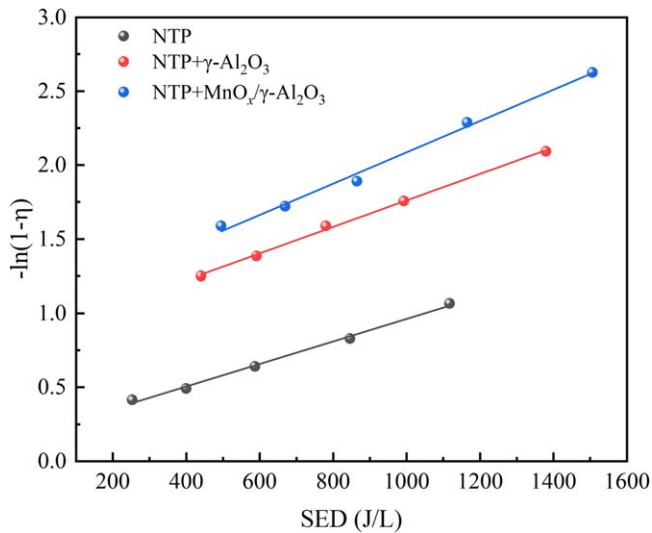$$-\frac{dc_{CB}}{dt} = k' \cdot c_{CB} \cdot SED \tag{12}$$

Figure 13. Kinetics analysis of CB degradation using NTP coupled with catalyst.

$$- \ln\left(\frac{c_{\text{out}}}{c_{\text{in}}}\right) = k' \cdot \text{SED} \cdot t \qquad (13)$$

$$- \ln\left(1 - \eta\right) = k_{\text{overall}} \cdot \text{SED}, \qquad (14)$$

where c_{CB} is the CB concentration, mg m^{-3}; R_{overall} is the overall reaction rate of CB in plasma, mg m^{-3} s^{-1}; k' is the rate constant, s^{-1}; c_{in} is the initial concentration of CB, mg m^{-3}; c_{out} is the outlet concentration of the CB after DBD treatment, mg m^{-3}; t is the residence time of a gas in the system, s; and k_{overall} is the overall energy constant of CB degradation reaction, ml J^{-1}.

Figure 13 depicts the linear relationship between $\ln(1-\eta)$ and SED in different reaction systems. Further, the total energy constant k_{overall} for different reaction systems could be obtained using the slope of the fitting curves. The results demonstrated that the linear fittings were statistically acceptable due to the regression coefficients (R^2) of the fitting curves in all reaction systems being higher than 0.99 (as shown in table 3). The system of NTP coupled with the MnO$_x$/γ-Al$_2$O$_3$ catalyst had the highest k_{overall} value for CB degradation, which is consistent with the degradation performance of CB (as shown in figure 8(b)).

3.4.2. Interactions between plasma and the catalyst. In the NTP-coupled catalytic reaction system, the interactions between plasma and catalysts could affect the reaction process of plasma catalysis. In the IPC reaction system, the catalyst was placed in the discharge area, which affected the discharge behavior of the plasma [70, 71]. On one hand, the catalysts affected the plasma discharge behavior. Figure 13(a) shows the discharge image of the NTP and IPC reaction system at 18 kV. It can be seen that the discharge phenomenon of the NTP system was mainly concentrated near the discharge electrode, while the discharge phenomenon of the IPC reaction system fills the entire discharge area (the schematic of the discharge is shown in figure 14(b)); the surface discharge phenomenon could be generated by the
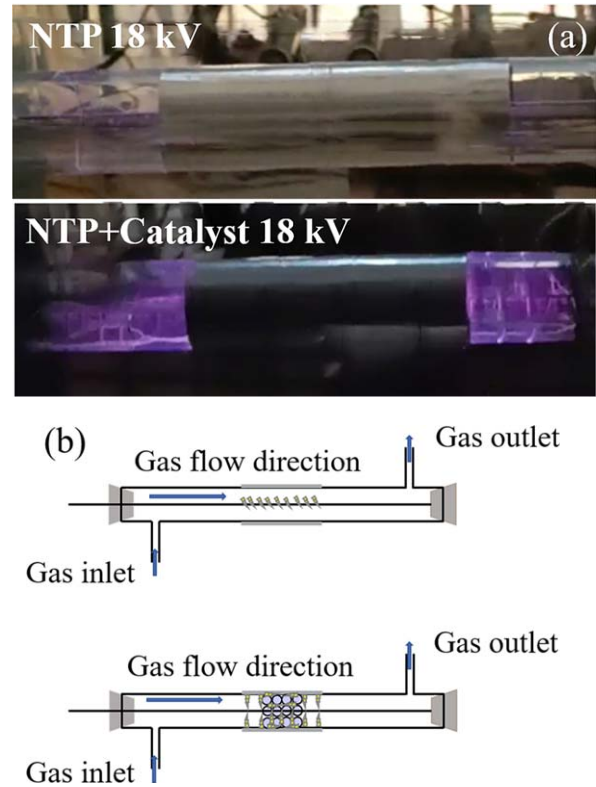

Figure 14. (a) Discharge images of NTP and IPC systems at 18 kV, (b) schematic diagram of the discharge.

Table 3. Overall energy constant (k_{overall}), standard error and regression coefficient (R^2) for different reaction systems.

	NTP	NTP + γ-Al$_2$O$_3$	NTP + MnO$_x$/γ-Al$_2$O$_3$
k_{overall} (ml J^{-1})	0.762	0.895	1.06
Standard error	2.878×10^{-5}	2.26×10^{-5}	5.14×10^{-5}
R^2	0.994	0.997	0.991

plasma along the catalyst surface, and the discharge channel was closed to the catalyst surface and extended outward. Further, the enhanced ionization effect along the catalyst surface contributed to the effective utilization of the active species on the catalyst surface [72] (as shown in figure 14(b)). On the other hand, the physical and chemical properties of the catalyst were changed by NTP. To investigate the influence of NTP on the catalyst, the used catalyst was characterized and analyzed. The results indicated that the crystalline phase structure (figures 3(a) and (b)) and pore structure (figure 4) of the catalyst were not destroyed by high voltage discharge, however, the surface morphology (figure 5) of the catalyst was altered. The XPS (figure 6) results of the used catalyst showed that the existing form of the metal oxide in the catalyst remained unchanged. However, in comparison to the fresh catalyst, the Mn^{4+} ratio of the used catalyst decreased from 21.88% to 18.25%, while the surface oxygen decreased from 20.07% to 15.93%; the former was mainly attributed to the decomposition of ozone on the catalyst surface, and the
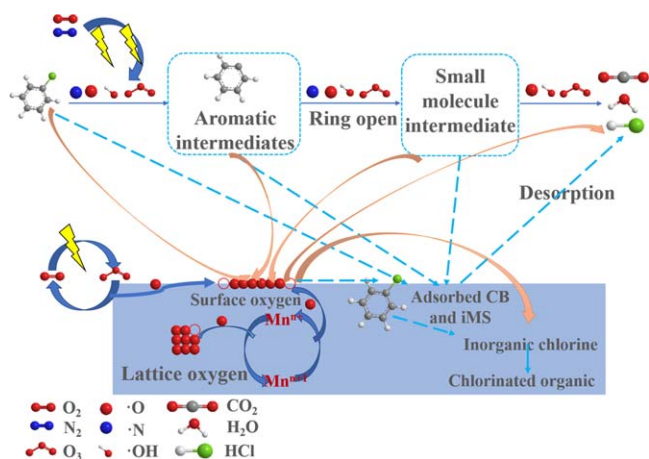
Figure 15. General reaction mechanism of CB degradation in an IPC reaction system.

surface oxygen participated in the degradation of CB [73]. Therefore, the physical properties of the fresh and used catalyst remained basically unchanged, but the surface morphology was altered, and the chemical properties exhibited slight changes. In general, plasma discharge characteristics played a major role in the NTP synergistic catalytic degradation of CB. The introduction of the catalyst changed the discharge mode of the reaction system and enhanced the discharge intensity; however, the activity of the catalyst in the NTP reaction system was not well-reflected.

3.4.3. Synergistic mechanism of degradation of CB by NTP with catalyst. In this research, the decomposition mechanism proposed could be divided into two parts: the gas phase reaction and catalyst surface reaction [74, 75]. According to the actual experimental conditions, the general reaction mechanism of CB degradation in the IPC reaction system was proposed, as shown in figure 15.

The gas-phase reaction process of the NTP degradation of CB was mainly divided into two types, one was the direct collision between high-energy electrons generated in the discharge process and CB molecules, and the other was the interaction between gas-phase free radicals (such as O·, ·OH, O_3, etc) generated in the discharge process and CB molecules [76]. In the process of plasma discharge, the energy obtained by electrons is between 2 and 20 eV, and the maximum energy distribution probability ranged from 2 to 12 eV [64]. In CB molecules, the bond energy of the C–Cl bond on its branched chain was 4.2 eV, which was less than that of the C–H bond (4.4 eV), C–C bond (5.0–5.3 eV), and C=C bond (5.5 eV) [77–79]. Therefore, the destruction of the C–Cl bond on its branched chain was the easiest process in CB decomposition, which leads to the formation of a phenyl radical (as shown in equation (15)). Further, the production of inorganic chlorine could also verify this result (with discharge voltage increase from 14 to 22 kV, the selectivity of Cl^{-1} increasing from 4.4% to 12.5% under the condition of NTP alone). Further, many aromatic intermediates and CO_2 were produced

$$C_6H_5Cl + e \rightarrow C_6H_5· + Cl· \qquad (15)$$
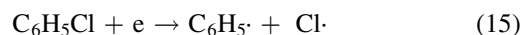
As a polar molecule, CB has strong adsorption performance. Thus, CB, intermediates, and active particles were adsorbed on the catalyst surface in the IPC system, but the plasma in the coupling systems had a great influence on the adsorption–desorption equilibrium of the catalyst surface [80], and the collision of high-energy electrons could promote the dissociation chemisorption process of the catalyst surface [81]. Moreover, the active oxygen species of the catalyst surface could not only react with the CB adsorbed on the catalyst surface (Langmuir-Hinshelwood mechanism), but also with CB molecules in the gas phase (Eley-Rideal mechanism). The formation of active oxygen species had three pathways. Firstly, high-energy electrons bombard oxygen molecules (as shown in equation (5)). Secondly, ozone decomposes on the catalyst surface. Thirdly, in the MnO_x catalyst, the change of the valence state of the Mn element could lead to the transmission of oxygen species (Mars-van Krevelen mechanism). This is further oxidized to CO_2, H_2O, and inorganic chlorine; therefore, the degradation efficiency of CB and CO_2 selectivity in the IPC reaction system were improved.

4. Conclusion

The effects of the catalyst and the locations of the catalyst in the NTP on the degradation of CB have been investigated in this study. In comparison to the process of only NTP, the introduction of the catalyst improved the degradation efficiency of CB, EE, CO_2 selectivity, and inhibited the formation of ozone, and the MnO_x/γ-Al_2O_3 catalyst obtained the optimal degradation performance, which was mainly attributed to the formation of more reactive species from high-energy electrons and ozone decomposition. Further, the degradation efficiency of IPC systems was better than that of the PPC system, while the inhibition ability of ozone had opposing results. The characterization of fresh and used γ-Al_2O_3 and MnO_x/γ-Al_2O_3 catalysts demonstrated that plasma will not destroy the pore structure and crystal structure of the catalyst, but will affect the surface morphology and redox performance of the catalyst. Further research showed that the plasma discharge characteristics played a major role in the NTP synergistic catalytic degradation of CB. Finally, based on the experimental analysis results, it was proposed that the catalyst follows the Langmuir-Hinshelwood, Eley-Rideal and Mars-van Krevelen mechanism in the process of the NTP synergistic catalytic degradation of CB.

Acknowledgments

References

[1] Lyu X *et al* 2020 *Chemosphere* **246** 125731
[2] Liu B Y *et al* 2022 *J. Hazard. Mater.* **422** 126847
[3] Chang T *et al* 2021 *Plasma Chem. Plasma Process.* **41** 1239
[4] Lin F W *et al* 2021 *Chem. Eng. J.* **404** 126534
[5] Zhang S H *et al* 2018 *Chem. Eng. J.* **334** 2625
[6] Qian Y *et al* 2004 *Chemosphere* **57** 127
[7] Jin X P *et al* 2021 *Appl. Sci.* **11** 6433
[8] Hu Y X *et al* 2022 *J. Mater. Sci.* **57** 1536
[9] Liang W J *et al* 2021 *Appl. Catal.* A **623** 118257
[10] Li B *et al* 2020 *Sci. Total Environ.* **749** 141595
[11] Deng W *et al* 2020 *Appl. Catal.* B **278** 119336
[12] Li S J *et al* 2021 *J. Environ. Chem. Eng.* **9** 106562
[13] Weng X L *et al* 2020 *J. Hazard. Mater.* **387** 121705
[14] Zou W X *et al* 2019 *Chemosphere* **218** 845
[15] Han F L *et al* 2020 *J. Saudi. Chem. Soc.* **24** 673
[16] Chang Z S *et al* 2020 *Plasma Process Polym.* **17** 1900131
[17] Nguyen V T *et al* 2020 *Plasma Chem. Plasma Process.* **40** 1207
[18] Saoud W A *et al* 2019 *Appl. Catal.* B **241** 227
[19] Neyts E C *et al* 2015 *Chem. Rev.* **115** 13408
[20] Yu X *et al* 2020 *J. Clean. Prod.* **276** 124251
[21] Whitehead J C 2016 *J. Phys. D: Appl. Phys.* **49** 243001
[22] Fan H Y *et al* 2011 *Plasma Chem. Plasma Process.* **31** 799
[23] Pan K L and Chang M B 2019 *Environ. Sci. Pollut. Res.* **26** 12948
[24] Jia Z X *et al* 2017 *Plasma Process Polym.* **14** 1600114
[25] Ogata A *et al* 2010 *Plasma Chem. Plasma Process.* **30** 33
[26] Yao X H *et al* 2019 *Chemosphere* **230** 479
[27] Chang T *et al* 2018 *Chem. Eng. J.* **348** 15
[28] Sivachandiran L *et al* 2015 *Chem. Eng. J.* **270** 327
[29] Liu Y H C *et al* 2020 *Plasma Sci. Technol.* **22** 034016
[30] Zheng B *et al* 2019 *RSC Adv.* **9** 7447
[31] Xie W *et al* 2022 *J. Hazard. Mater.* **440** 129751
[32] Wang L *et al* 2016 *Chem. Eng. J.* **288** 406
[33] Wu Z L *et al* 2020 *IEEE Trans. Plasma Sci.* **48** 163
[34] Wang B W *et al* 2017 *Chem. Eng. J.* **322** 679
[35] He D D *et al* 2017 *Catal. Today* **281** 559
[36] Allahyari S *et al* 2014 *Ultrason. Sonochem.* **21** 663
[37] Gholipour A M *et al* 2017 *Top. Catal.* **60** 934
[38] Das Neves Gomes C *et al* 2012 *Angew. Chem. Int. Ed.* **51** 1
[39] Li Y Z *et al* 2014 *Chem. Eng. J.* **241** 251
[40] Hoseini S *et al* 2019 *J. Clean. Prod.* **232** 1134
[41] Feng X B *et al* 2020 *J. Hazard. Mater.* **383** 121143
[42] Li L M, Chu W and Liu Y 2021 *J. Mater. Sci.* **56** 6361
[43] Liang C F *et al* 2019 *Int. J. Hydrogen. Energ.* **44** 8197
[44] Xiao G *et al* 2014 *Plasma Chem. Plasma Process.* **34** 1033
[45] Zhang H *et al* 2010 *Fuel* **89** 3127
[46] Fang R M *et al* 2018 *Chem. Eng. J.* **334** 2050
[47] Li H W *et al* 2017 *Chem. Eng. J.* **316** 61
[48] Guo H *et al* 2019 *Environ. Sci. Pollut. Res.* **26** 8237
[49] Wang T *et al* 2017 *Chin. J. Catal.* **38** 793
[50] Chen Y X *et al* 2017 *Environ. Sci. Technol.* **51** 2304
[51] Yang X Q *et al* 2017 *J. Mater. Chem.* A **5** 13799
[52] Tang X F *et al* 2006 *Appl. Catal.* B **62** 265
[53] Yodsanga A *et al* 2015 *Surf. Coat. Technol.* **271** 217
[54] Zhang X *et al* 2021 *Sep. Purif. Technol.* **257** 117973
[55] Liu X *et al* 2021 *Chemosphere* **284** 131299
[56] Vandenbroucke A M *et al* 2011 *J. Hazard. Mater.* **195** 30
[57] Li S J *et al* 2020 *J. Hazard. Mater.* **400** 123259
[58] Kim H H *et al* 2006 *IEEE Trans. Plasma Sci.* **34** 984
[59] Huang H *et al* 2020 *Appl. Surf. Sci.* **503** 144290
[60] Huu T P *et al* 2015 *Catal. Today* **257** 86
[61] Paulussen S *et al* 2010 *Plasma Sources Sci. Technol.* **19** 034015
[62] Liu J Q *et al* 2021 *Catalysis* **11** 828
[63] Maciuca A *et al* 2012 *Appl. Catal.* B **125** 432
[64] Wang M X *et al* 2014 *Chin. J. Catal.* **35** 335
[65] Feng X X *et al* 2018 *Catal. Sci. Technol.* **8** 936
[66] An H T Q *et al* 2011 *Catal. Today* **176** 474
[67] Nie Y N *et al* 2022 *Chemosphere* **303** 135184
[68] Huang H B *et al* 2011 *IEEE Trans. Plasma Sci.* **39** 576
[69] Zhu X B *et al* 2015 *Catal. Today* **256** 108
[70] Tu X *et al* 2012 *Appl. Catal.* B **125** 439
[71] Mei D H *et al* 2015 *Plasma Sources Sci. Technol.* **24** 015011
[72] Kim H H *et al* 2009 *J. Phys. D: Appl. Phys.* **42** 135210
[73] Zeng X B *et al* 2017 *Chem. Eng. J.* **309** 503
[74] Zhu X B *et al* 2015 *Appl. Catal.* B **170** 293
[75] Lu M J *et al* 2015 *Catal. Today* **242** 274
[76] Liang W J *et al* 2013 *Chemosphere* **92** 1390
[77] Li L *et al* 2021 *Appl. Catal.* B **282** 119565
[78] Zhou W *et al* 2021 *J. Clean. Prod.* **288** 125502
[79] Xie L X *et al* 2022 *Environ. Technol.* **43** 2743
[80] Blin-Simiand N *et al* 2005 *Plasma Process. Polym.* **2** 256
[81] Nozaki T *et al* 2007 *Energy Fuels* **21** 2525